

650 years. (Cooling was stopped when fragmentation was approached.)
 32. K. L. Luhman, R. Jayawardhana, *Astrophys. J.* **566**, 1132 (2002).
 33. E. W. Thommes, M. J. Duncan, H. F. Levison, *Astron. J.* **123**, 2862 (2002).

34. J. Stadel, J. Wadsley, D. Richardson, in *High Performance Computing Systems and Applications*, M. J. Dimopoulos, K. F. Lie, Eds. (Kluwer Academic, Boston, 2002), p. 501.
 35. The authors thank G. Laughlin, D. Hollenbach, and A. Boss for useful and stimulating discussions. Simulations were carried out at the Pittsburgh Supercom-

puting Center and at Consorzio Interuniversitario per il Calcolo Automatico dell'Italia Nord Orientale. This research was supported by a grant from the NSF and by the NASA Astrobiology Institute.

22 August 2002; accepted 4 November 2002

In Vivo Imaging of Quantum Dots Encapsulated in Phospholipid Micelles

Benoit Dubertret,^{1,3*†} Paris Skourides,² David J. Norris,^{3,4*} Vincent Noireaux,¹ Ali H. Brivanlou,² Albert Libchaber^{1,3}

Fluorescent semiconductor nanocrystals (quantum dots) have the potential to revolutionize biological imaging, but their use has been limited by difficulties in obtaining nanocrystals that are biocompatible. To address this problem, we encapsulated individual nanocrystals in phospholipid block-copolymer micelles and demonstrated both in vitro and in vivo imaging. When conjugated to DNA, the nanocrystal-micelles acted as in vitro fluorescent probes to hybridize to specific complementary sequences. Moreover, when injected into *Xenopus* embryos, the nanocrystal-micelles were stable, nontoxic ($<5 \times 10^9$ nanocrystals per cell), cell autonomous, and slow to photobleach. Nanocrystal fluorescence could be followed to the tadpole stage, allowing lineage-tracing experiments in embryogenesis.

Nanometer-scale semiconductor crystallites (known as nanocrystals or quantum dots) (1–3) could dramatically improve the use of fluorescent markers in biological imaging (4, 5). Because these colloidal particles act as robust, broadly tunable nanoemitters that can be excited by a single light source, they could provide distinct advantages over current in vitro and in vivo markers (e.g., organic dyes and fluorescent proteins). However, before nanocrystals can be widely used as biolabels, they must maintain three properties under aqueous biological conditions: efficient fluorescence, colloidal stability, and low nonspecific adsorption. Unfortunately, despite recent advances (4–12), these conditions have not been simultaneously satisfied, limiting the development of in vivo applications of nonaggregated (or individual) semiconductor nanocrystals.

The main challenge is that the quantum dots (QDs), as synthesized, have hydrophobic organic ligands coating their surface (2, 3). To make the QDs water soluble, these organophilic surface species are generally exchanged with

more-polar species, and both monolayer (5, 6) and multilayer (4) ligand shells have been pursued. Although the monolayer method is reproducible, rapid, and produces QDs with a regular, well-oriented, thin coating, their colloidal stability is poor (9). In contrast, the multilayer method yields QDs that are stable in vitro (8), but the coating process is long and the coating is difficult to control. A more serious concern is that both approaches still produce QDs that tend to aggregate and adsorb nonspecifically. To resolve this problem, researchers have explored two additional coatings. First, the outer ligand shell of the QD has been overcoated with proteins adsorbed through hydrophobic or ionic interactions (7). Other layers can then be added to allow conjugation with specific biomolecules. Indeed, this method has provided new reagents for fluoroimmunoassays (10). Second, the outer ligand shell has been overcoated with surfactants or polymers to prevent nonspecific adsorption of biomolecules while still permitting bioconjugation. For example, silica-coated QDs have been further modified with small monomers of poly(ethylene glycol) to reduce nonspecific adsorption (11).

Despite these efforts, nonspecific adsorption and aggregation still occur when QDs are used in biological environments. Studies of cellular uptakes of QDs report large aggregate formation inside the cell (5, 13). The same aggregation problems are reported when QDs are used for fluorescence in situ hybridization (14), or as markers for molecular recognition on cell surfaces (15, 16). Consequently, the use of QDs in biological

applications is still limited and primarily confined to in vitro studies.

We found, however, that without any surface modifications, individual ZnS-overcoated CdSe QDs (2, 3) could be encapsulated (17) in the hydrophobic core of a micelle composed of a mixture of *n*-poly(ethylene glycol) phosphatidylethanolamine (PEG-PE) and phosphatidylcholine (PC) (Fig. 1A). PEG-PEs are micelle-forming hydrophilic polymer-grafted lipids (18, 19) comparable to naturally occurring carriers such as lipoproteins and viruses (20). They have been used for drug delivery (21) and diagnostic imaging (22). The advantage of these micelles is that they are very regular in size, shape, and structure (23). In addition, their outer surface comprises a dense layer of PEG polymers that is poorly immunogenic and antigenic and acts as excellent repellent for biomolecules (24). Further, both the PEG content and length can be adjusted precisely.

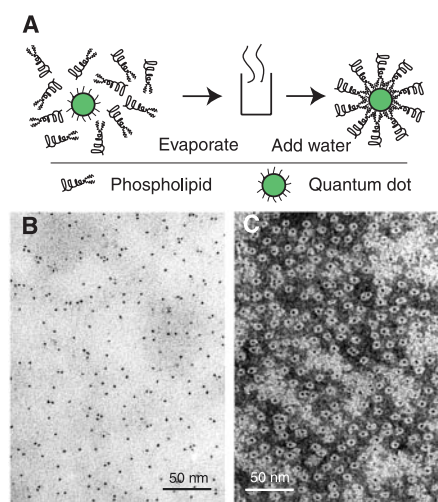


Fig. 1. QD-micelle formation and characterization. (A) Schematic of single-QD encapsulation in a phospholipid block-copolymer micelle. (B) TEM image of QD-micelles dried on a carbon-Formvar-coated 200-mesh nickel grid. Only the QDs inside the micelle core are visible. The particles appear evenly spread on the surface. Although some clusters of two to four QDs are visible, most of the QDs are isolated, suggesting that a majority of micelles contain a single QD. (C) TEM image of the phospholipid layer obtained by negative staining with 1% PTA (phosphotungstic acid) at pH 7. With this technique, both the QD and the micelle can be visualized at the same time. The QD (dark spot) appears surrounded by a white disk of unstained phospholipids that stands out against the stained background. A JEOL 100CX TEM was operated at 80 kV.

¹Center for Studies in Physics and Biology, ²Laboratory of Molecular Embryology, The Rockefeller University, 1230 York Avenue, New York, NY 10021, USA. ³NEC Research Institute, 4 Independence Way, Princeton, NJ 08540, USA. ⁴Department of Chemical Engineering and Materials Science, University of Minnesota, 421 Washington Avenue SE, Minneapolis, MN 55455, USA.

*To whom correspondence should be addressed. E-mail: benoit.dubertret@espci.fr, dnorris@umn.edu
 †Present address: UPRA0005, CNRS and ESPCI, Laboratoire d'Optique Physique, 10 rue Vauquelin, 75005 Paris, France.

REPORTS

By transmission electron microscopy (TEM), the QD-micelles appeared spherical and fairly monodisperse (Fig. 1, B and C).

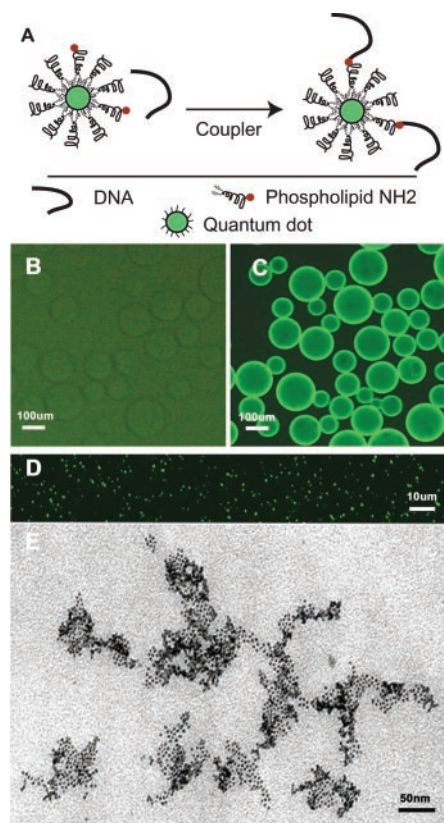


Fig. 2. Conjugation of QD-micelles with DNA. (A) Schematic of the QD-micelle conjugation with single-stranded DNA (ssDNA). (B and C) Hybridization of QD-micelles conjugated with DNA to surface-bound ssDNA. 5'-Biotin-modified ssDNA (5'-TTACTCGAGGGATCCTAGTC-3') was attached to streptavidin-modified 4% agarose beads. A PBS solution containing QD-micelles conjugated with 20-base-long ssDNA was added to the bead solution and incubated at room temperature for more than 10 min. After rinsing once with PBS, the bead fluorescence is measured with an optical microscope. In (B), the oligonucleotides bound to the agarose beads are not complementary to the oligonucleotides bound to the QD-micelle. In (C), they are complementary. (D) Fluorescence image of aggregates of DNA-QD-micelles obtained by mixing equal amounts of two batches of QD-micelles conjugated with complementary single-stranded oligonucleotides. (E) TEM image of the same sample as in (D). The fluorescence images were obtained with Chroma filter set 41015 (wild-type GFP longpass emission with a 50-nm-wide band-pass excitation centered at 450 nm) mounted on a Zeiss fluorescence microscope. The samples were excited with a 50-W mercury lamp. Images were recorded with a color digital camera (AxioCam HR, Zeiss) and AxioVision Viewer software (Zeiss). In all experiments the QDs had a 3.5-nm-diameter CdSe core and ZnS outer layer. These QDs absorb light with wavelengths <515 nm and emit light at ~ 550 nm. Their extinction coefficient is $8.4 \times 10^5 \text{ M}^{-1} \text{ cm}^{-1}$ (29).

Their size was measured between 10 and 15 nm; however, this range probably reflects the different conformations that the PEG molecule can adopt as the QD-micelles lay down on the TEM grid. In any event, the size is very similar to the diameter of empty micelles formed with 100% PEG-PE phospholipids previously measured in solution (23, 25). The encapsulation of the QD inside the micelle does not appreciably perturb its geometry or size. This is reasonable because, according to measurements of the micelle core (23), one would expect QDs with diameters <3 nm to fit loosely inside the micelle. QDs with diameters >3 nm should slightly overfill the micelle core and provide a solid hydrophobic surface that further stabilizes the structure. We observed that aqueous suspensions with 4-nm ZnS-overcoated CdSe QDs were stable for months (even in 1 M salt), whereas empty micelles degraded and formed aggregates after several days. Further, at 4 nm, the vast majority of QD-micelles con-

tained only one particle, while at smaller sizes (<3 nm) they contained multiple QDs, as one might expect. The fluorescence quantum yield of the 4-nm QD-micelles in water was 24% without any optimization.

The ability to encapsulate single QDs depended critically on the properties of the PEG-PE block-copolymer. Both the PEG block and the two alkyl chains linked to the PE block seem to be necessary. Surfactants with a single alkyl chain did not form single QD-micelles, even when they contained PEG [e.g., Brij78 (Sigma)]. Conversely, surfactants with two alkyl chains that lack PEG, like bis(2-ethylhexyl) sulfosuccinate (AOT), allowed single QDs to be suspended in water, but failed to prevent aggregation when salt was added to the solution. Micelles also failed to form when PC alone was used. However, with PEG-PE phospholipids, QD-micelles could be formed with various PEG lengths. QD-micelles similar in shape and stability were obtained from PEG chains with

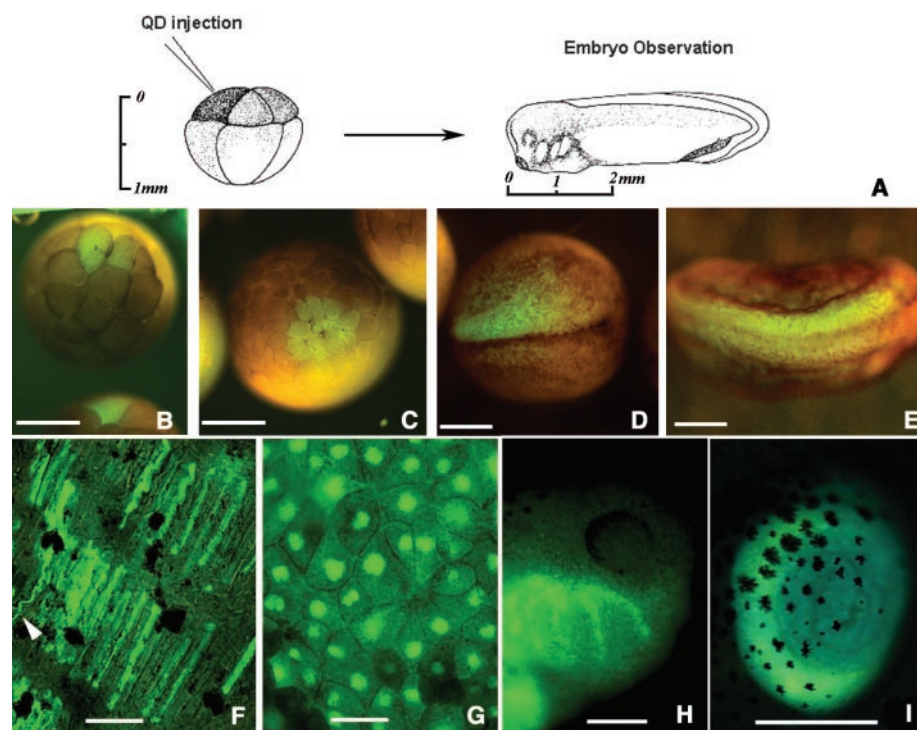


Fig. 3. QD labeling of *Xenopus* embryos at different stages and specific QD intracellular localizations. (A) Schematic showing the experimental strategy. QD-micelles, as in Fig. 2, were injected into an individual blastomere during very early cleavage stages. Between 1.5 and 3 nl of a $2.3 \mu\text{M}$ suspension of QDs were injected, corresponding to 2.1×10^9 to 4.2×10^9 injected particles per cell. Embryos were then cultured until they reached different stages of development, and imaging was done as in Fig. 2. In (B) to (E), transmission and fluorescence images have been superposed. (B) Injection of one cell out of an eight-cell-stage embryo resulted in labeling of individual blastomeres. (C) Same embryo shown 1 hour later. The daughter cells of the injected blastomere are labeled (D) and at a later stage (E) show two neurula embryos, which were injected into a single cell at the eight-cell-stage in the animal pole. The QDs can be visualized through the pigmented layer of the epidermis. (F) Intracellular labeling of an axon (arrow) and somites at tadpole stage 40. The QD-micelles migrate into axons all the way to growth cones. In the somites, the QD-micelle seems to localize in subcellular structures. (G) QDs localized in the nucleus during mid-blastula stages. This localization is reduced in later stages of the development. (H) Labeled neural crest cells migrating into the branchial arches. (I) QD fluorescence observed in the gut of an injected embryo. Bars: (B) to (E), (H), and (I), 0.5 mm; (F) and (G), 30 μm .

REPORTS

molecular weights of 550, 2000, and 5000. The results reported here are for PEG-2000.

The QD-micelles could be attached to DNA by replacing up to 50% of the PEG-PE phospholipids with an amino PEG-PE during the micelle formation, thus introducing a primary amine to the outer surface of the micelle. Thiol-modified DNA was then covalently coupled to the amines using a heterobifunctional coupler, with noncoupled DNA removed by ultracentrifugation (17). As illustrated in Fig. 2A, the DNA was coupled at the outer end of the PEG molecule. This geometry is optimal both to preserve the availability of the DNA for hybridization and to give efficient coupling. Oligonucleotide-QD-micelles were shown to bind specifically to cDNA, immobilized in 4% agarose beads, but not to noncomplementary oligonucleotides (Fig. 2, B and C). This demonstrates that QD-micelles attached to the oligonucleotides do not prevent their specific hybridization to DNA targets. This process was also very rapid, because incubation times as low as 10 min yielded highly fluorescent agarose beads (Fig. 2C).

These results compare favorably with those from silica-coated QDs. Our fluorescence signal-to-background ratio was >150 , compared with about 4 for silica-coated QDs (11), due to the low nonspecific adsorption offered by the PEG-2000. After a single wash with phosphate-buffered saline (PBS), we observed no fluorescence in the agarose beads decorated with nonspecific targets (Fig. 2B). In addition, our approach offers excellent conjugation yields.

When the number of DNA-QD-micelles was less than the number of binding sites, all QD-micelles were immobilized in the agarose beads, suggesting that at least one DNA molecule was linked to each micelle. Moreover, compared to silica-coated QDs (11), our QD-micelles are viable over a much broader range of QD and salt concentration.

To verify further the efficiency of the hybridization of DNA-QD-micelle conjugates to complementary sequences, we also performed directed assembly (26, 27). We mixed equal amounts of two batches of QD-micelles, each conjugated with a complementary oligonucleotide. After a 1-hour incubation at room temperature, fluorescent aggregates were visible under the microscope (Fig. 2D). TEM confirmed that these aggregates, which ranged in size from 0.2 to 2 μm , were formed from QD-micelles (Fig. 2E).

These successful experiments in vitro prompted us to investigate QD-micelles in vivo. Synthetic fluorophores or fluorescent proteins are currently used as tracers for in vivo imaging. However, these approaches are restricted by photobleaching and the limited availability of different colors. QD-micelles offer an attractive alternative, but two criteria must be met. The QD-micelles must be biologically neutral (i.e., no biological activity or toxicity), and they must be stable for long periods of time. To address these issues, we performed in vivo imaging with QD-micelles by microinjecting early-stage *Xenopus* embryos (Fig. 3A). An embryo is a sensitive test

environment for biological activity and toxicity because cellular perturbances are manifested as measurable biological phenotypes. We chose *Xenopus* because a large number of embryos could be easily obtained, allowing a statistical analysis of different parameters.

Figure 3 shows QD-micelles injected into individual cells of an early embryo. Several key results are noted: (i) The QD-micelles were cell autonomous. When one cell from a two-cell embryo was injected, the QD fluorescence was confined to the progeny of the injected cell (i.e., only half of the embryo was fluorescently labeled). When injected later in embryogenesis into individual blastomeres, the QDs were similarly confined only to the progeny of the injected cells during development (Fig. 3, B to E). (ii) The QD-micelles seemed to have very little activity or toxicity. The toxicity was sufficiently low that cell lineage could be traced by fluorescence visualization. For typical QD injections (2×10^9 QDs/cell), injected embryos displayed an unaltered phenotype and their health was statistically similar to that of uninjected embryos (Table 1). At higher injection concentrations ($>5 \times 10^9$ QDs/cell), abnormalities became apparent. The cause of these defects is not yet known, but may result from changes in the osmotic equilibrium of the cell. (iii) The QD-micelles were stable in vivo. The fluorescence signal remained detectable throughout the experiment despite a restriction of the signal after the tailbud stage (we observed up to late tadpole stages). In addition, after 4 days of embryonic development, the QD-micelles did not exhibit any visible aggregation. (iv) The QD-micelle could label all embryonic cell types, including somites, neurons and axonal tracks (Fig. 3F), ectoderm (Fig. 3G), neural crest (Fig. 3H), and endoderm (Fig. 3I) without visible segregation. (v) The QD fluorescence was visible very early during development (Fig. 3B) despite pigmentation and

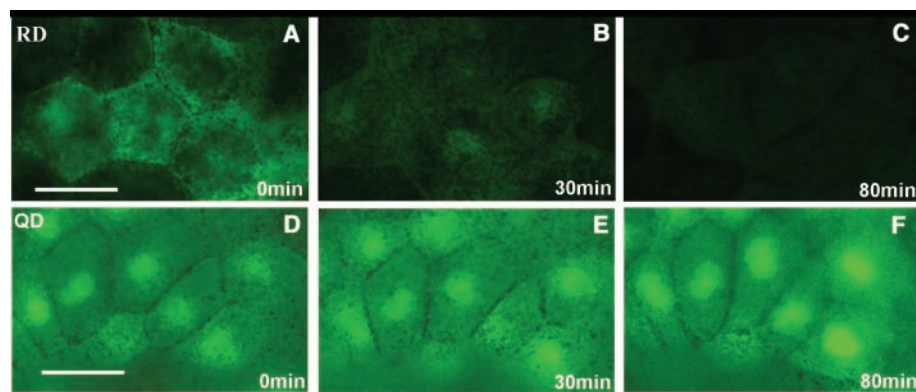


Fig. 4. Comparison of QD and RG-D (Rhodamine Green Dextran, Molecular Probes) for resistance to photobleaching. QDs and injection amounts are similar to those used in Fig. 3. For RG-D, 1 nl of a 25 mg/ml solution was injected. (A to C) Consecutive images of RG-D-injected *Xenopus* animal pole blastomeres. (D to F) Consecutive images of QD-injected *Xenopus* animal pole blastomeres. During each experiment, the injected embryos were excited continuously at 450 nm. (G) Graph representing the variation of fluorescence intensity of one cell of the RG-D-injected embryo (dotted line) and of one cell of the QD-injected embryo (solid line). Bars, 30 μm . The optical setup is as described in Fig. 2.

Table 1. Toxicity of 1.5-nl animal pole QD injections (QD concentration: 2.3 μM). *Xenopus* embryos were injected at the eight-cell-stage, and the QDs were delivered to one of the four animal pole cells. Toxicity was assessed by close examination of the injected embryos under a dissecting microscope, and normal embryos were scored only if absolutely no phenotypical abnormalities were present. Because of the strict criteria used, a high percentage of abnormal embryos in both control (uninjected) and injected embryos were recorded. In the case of QD injections, defective embryos showed a range of abnormalities including cell size, cell death, cell movement, and axis elongation. Occasional axis duplications and posterior truncations were also observed.

Stage 19–20 embryos	QD injections (n = 55)	Control (n = 39)
Normal	38 (69%)	27 (69%)
Defective	15 (27%)	12 (31%)
Dead	2 (4%)	0 (0%)

strong background fluorescence. In contrast, injection of green fluorescent protein (GFP) as a tracer (e.g., by injection of RNA that encodes GFP) requires time for GFP to be expressed at levels detectable *in vivo*. (vi) Examination of the embryos at tadpole stages also showed that strong QD fluorescence was visible even in high-background regions such as the embryo gut (Fig. 3, H and I). (vii) The QD-micelles were much more resistant to photobleaching than were other fluorophores *in vivo*, which has been shown previously *in vitro* (4). Figure 4 compares the *in vivo* fluorescence quenching of QD-micelles and rhodamine green-dextran (RG-D). QD-micelles and RG-D were microinjected into sibling embryos that were at similar stages of development and had progressed to late blastula when they were imaged by time-lapse microscopy. After 80 min of constant illumination (at 450 nm) under the microscope, the QD fluorescence intensity remained unchanged (Movie S1), whereas the dextran had photobleached. Experiments with a membrane-bound GFP (EGFP fused to the Ras farnesylation sequence) gave similar results, with the QDs showing increased stability (fig. S1).

Although at early embryonic stages, QDs appeared to be diffusely localized throughout the cell, at later stages they concentrated in the cell nuclei (Fig. 3G). Time-lapse microscopy (Movies S2 and S3) revealed that this translocation to the nucleus occurs at a stage that phenotypically resembles the mid-blastula transition (MBT) (28), a critical stage in amphibian development when zygotic gene transcription is initiated. Because QD-micelles do not bind to DNA directly, it would be interesting to explore the mechanism of this translocation. If translocation proves to be concomitant with MBT, QDs will enable us to observe MBT *in vivo* with single-cell resolution.

These results indicate that micelle-encapsulated QDs fulfill the promise of fluorescent semiconductor nanocrystals for both *in vitro* and *in vivo* studies. Compared to other systems, they simultaneously provide efficient fluorescence, a great reduction in photobleaching, colloidal stability in a variety of bioenvironments, and low nonspecific adsorption.

References and Notes

- A. P. Alivisatos, *Science* **271**, 933 (1996).
- C. B. Murray, D. J. Norris, M. G. Bawendi, *J. Am. Chem. Soc.* **115**, 8706 (1993).
- M. A. Hines, P. Guyot-Sionnest, *J. Phys. Chem.* **100**, 468 (1996).
- M. Bruchez, M. Moronne, P. Gin, S. Weiss, A. P. Alivisatos, *Science* **281**, 2013 (1998).
- W. C. W. Chan, S. Nie, *Science* **281**, 2016 (1998).
- F. Mikulec, thesis, Massachusetts Institute of Technology (1999).
- H. Mattoussi *et al.*, *J. Am. Chem. Soc.* **122**, 12142 (2000).
- D. Gerion *et al.*, *J. Phys. Chem. B* **105**, 8861 (2001).
- J. Aldana, Y. A. Wang, X. G. Peng, *J. Am. Chem. Soc.* **123**, 8844 (2001).
- E. R. Goldman *et al.*, *Anal. Chem.* **74**, 841 (2002).
- D. Gerion *et al.*, *J. Am. Chem. Soc.* **124**, 7070 (2002).
- W. J. Parak *et al.*, *Adv. Mater.* **14**, 882 (2002).
- M. Dahan *et al.*, *Opt. Lett.* **26**, 825 (2001).
- S. Pathak, S. K. Choi, N. Arnheim, M. E. Thompson, *J. Am. Chem. Soc.* **123**, 4103 (2001).
- J. O. Winter, T. Y. Liu, B. A. Korgel, C. E. Schmidt, *Adv. Mater.* **13**, 1673 (2001).
- S. J. Rosenthal *et al.*, *J. Am. Chem. Soc.* **124**, 4586 (2002).
- Materials and methods are available as supporting material on Science Online.
- K. Hristova, D. Needham, *Macromolecules* **28**, 991 (1995).
- S. Belsito, R. Bartucci, G. Montesano, D. Marsh, L. Sportelli, *Biophys. J.* **78**, 1420 (2000).
- K. Kataoka, G. S. Kwon, M. Yokoyama, T. Okano, Y. Sakurai, *J. Control. Release* **24**, 119 (1993).
- M. C. Jones, J. C. Leroux, *Eur. J. Pharm. Biopharm.* **48**, 101 (1999).
- V. P. Torchilin, *Adv. Drug Delivery Rev.* **54**, 235 (2002).
- M. Johansson, P. Hansson, K. Edwards, *J. Phys. Chem. B* **105**, 8420 (2001).
- C. G. Golander *et al.*, in *Poly(ethylene glycol) Chemistry*, J. M. Harris, Ed. (Plenum, New York, 1992), p. 221.
- D. D. Lasic, M. C. Woodle, F. J. Martin, T. Valentincic, *Period. Biol.* **93**, 287 (1991).
- C. A. Mirkin, R. L. Letsinger, R. C. Mucic, J. J. Storhoff, *Nature* **382**, 607 (1996).
- A. P. Alivisatos *et al.*, *Nature* **382**, 609 (1996).
- J. Newport, M. Kirschner, *Cell* **30**, 675 (1982).
- C. A. Leatherdale, W.-K. Woo, F. V. Mikulec, M. G. Bawendi, *J. Phys. Chem.* **106**, 7619 (2002).
- We thank H. Shio for assistance with electron microscopy and R. Harland (University of California, Berkeley) for membrane-GFP constructs. B.D. was supported in part by the Norman and Rosita Winston Fellowship. V.N. was supported in part by the Burroughs Wellcome Foundation. P.S. and A.H.B. are supported by funds from the Steinbach Fund and the Rockefeller University. B.D. acknowledges discussions with S. M. Simon and J. K. Jaiswal.

Supporting Online Material
www.sciencemag.org/cgi/content/full/298/5599/1759/DC1
 Materials and Methods
 Fig. S1
 Movies S1 to S3

9 August 2002; accepted 28 October 2002

Guest-Dependent Spin Crossover in a Nanoporous Molecular Framework Material

Gregory J. Halder,¹ Cameron J. Kepert,^{1*} Boujemaa Moubaraki,² Keith S. Murray,² John D. Cashion³

The nanoporous metal-organic framework $\text{Fe}_2(\text{azpy})_4(\text{NCS})_4(\text{guest})$ (azpy is *trans*-4,4'-azopyridine) displays reversible uptake and release of guest molecules and contains electronic switching centers that are sensitive to the nature of the sorbed guests. The switching of this material arises from the presence of iron(II) spin crossover centers within the framework lattice, the sorbed phases undergoing "half-spin" crossovers, and the desorbed phase showing no switching property. The interpenetrated framework structure displays a considerable flexibility with guest uptake and release, causing substantial changes in the local geometry of the iron(II) centers. The generation of a host lattice that interacts with exchangeable guest species in a switchable fashion has implications for the generation of previously undeveloped advanced materials with applications in areas such as molecular sensing.

The self-organization of molecular species is fundamental to the generation of nanoscale molecular architectures that have specific structures and functions (1, 2). In the area of porous metal-organic frameworks, the structural versatility of molecular chemistry has allowed the rational design and assembly of materials having novel topologies and exceptional host-guest properties (3–8). There has been comparatively little attention, however, on exploiting the many unique electronic aspects of molecular chemistry to impart specific electronic function to these materials. We report here on the incor-

poration of electronic switches, in the form of spin crossover centers, into porous molecular framework lattices.

Spin crossover centers are a well-known form of molecular switch in which a change in the electronic configuration at a metal center (high-spin \leftrightarrow low-spin) leads to distinctive changes in molecular geometry, color, and magnetism (9). The phenomenon may be stimulated by electromagnetic radiation or by variation of temperature and/or pressure. The generation of cooperative systems that display metastability and therefore hysteresis, including with light-induced excited spin state trapping (10), has drawn attention to the use of spin crossover centers in areas such as data storage and displays (11). An important approach for achieving cooperative interactions, both steric and magnetic, is the direct molecular linkage of metal sites in supramolecular (12, 13) and framework (14–21) sys-

¹School of Chemistry, University of Sydney, Sydney, NSW 2006, Australia. ²School of Chemistry, Post Office Box 23, ³School of Physics and Materials Engineering, Post Office Box 27, Monash University, Melbourne, VIC 3800, Australia.

*To whom correspondence should be addressed. E-mail: c.kepert@chem.usyd.edu.au